Durham University

Durham Research Online

Deposited in DRO:

28 July 2016

Version of attached file:

Accepted Version

Peer-review status of attached file:

Peer-reviewed

Citation for published item:

Armstrong, Howard A. and Wagner, Thomas and Herringshaw, Liam G. and Farnsworth, Alexander J. and Lunt, Daniel J. and Harland, M. and Imber, Jonathan and Loptson, Claire and Atar, Elizabeth F.L. (2016) 'Hadley circulation and precipitation changes control black shale deposition in the Late Jurassic Boreal Seaway.', Paleoceanography., 31 (8). pp. 1041-1053.

Further information on publisher's website:

http://dx.doi.org/10.1002/2015PA002911

Publisher's copyright statement:

© 2016. The Authors. This is an open access article under the terms of the Creative Commons Attribution License, which permits use, distribution and reproduction in any medium, provided the original work is properly cited.

Additional information:

Use policy

The full-text may be used and/or reproduced, and given to third parties in any format or medium, without prior permission or charge, for personal research or study, educational, or not-for-profit purposes provided that:

- a full bibliographic reference is made to the original source
- a link is made to the metadata record in DRO
- the full-text is not changed in any way

The full-text must not be sold in any format or medium without the formal permission of the copyright holders.

Please consult the full DRO policy for further details.

Durham University Library, Stockton Road, Durham DH1 3LY, United Kingdom
Tel : +44 (0)191 334 3042 | Fax : +44 (0)191 334 2971
https://dro.dur.ac.uk

Hadley circulation and precipitation changes control black shale deposition in the Late Jurassic Boreal Seaway

*Howard A. Armstrong[1], Thomas Wagner[2], Liam G. Herringshaw[1, 3], Alex Farnsworth[4], Daniel J. Lunt[4], Melise Harland[5], Jonathan Imber[1], Claire Loptson[4], Elizabeth Atar[1]

[1] Durham University, Department of Earth Science, Lower Mountjoy, South Road, Durham DH1 3LE, UK.

[2] Lyell Centre, Heriot-Watt University, Edinburgh, EH14 4AS, United Kingdom

[3] Department of Geography, Environmental and Earth Sciences, University of Hull, Hull, HU6 7RX, UK.

[4] School of Geographical Sciences and the Cabot Institute, University of Bristol, University Road, Bristol, BS8 1SS, UK.

[5] Getech, Kitson House, Elmete Hall, Elmete Lane, LEEDS, LS8 2LJ, UK.

*Corresponding author: h.a.armstrong@durham.ac.uk

Key points

- Late Jurassic ITCZ at mid-temperate latitudes
- Kimmeridge Clay deposition [35° to 54°N] was controlled by tropical climate
- Organic carbon and clay patterns support strong orbital contrasts in humidity

Abstract

[1] New climate simulations using the HadCM3L model with a paleogeography of the Late Jurassic [155.5 Ma], and proxy-data corroborate that warm and wet tropical-like conditions reached as far north as the UK sector of the Jurassic Boreal Seaway [~35°N]. This is

associated with a northern hemisphere Jurassic Hadley cell and an intensified subtropical jet which both extend significantly polewards than in the modern (July-September). Deposition of the Kimmeridge Clay Formation [KCF] occurred in the shallow, storm-dominated, epeiric Boreal Seaway. High resolution paleo-environmental proxy data from the Kimmeridge Clay Formation [KCF; ~155–150 Ma], UK are used to test for the role of tropical atmospheric circulation on meter-scale heterogeneities in black shale deposition. Proxy and model data show that the most organic-rich section [*eudoxus* to mid-*hudlestoni* zones] is characterised by a positive $\delta^{13}C_{org}$ excursion and up to 37 wt% total organic carbon [%TOC]. Orbital-modulation of organic carbon burial primarily in the long eccentricity power band combined with a clear positive correlation between %TOC carbonate-free and the kaolinite/illite ratio supports peak organic carbon burial under the influence of very humid climate conditions, similar to the modern tropics. This re-interpretation of large-scale climate relationships, supported by independent modelling and geological data, has profound implications for atmospheric circulation patterns and processes affecting marine productivity and organic carbon burial further north along the Boreal Seaway, including the Arctic.

Index Terms. 1600 Global Change

Keywords. Hadley Cell circulation; Kimmeridge Clay; black shale; Global climate simulation; proto-Arctic Ocean

1. Introduction

[2] Black shales represent major perturbations in the global carbon cycle and are recurrent throughout the Phanerozoic. At the present day, organic carbon [OC] rich sediments are largely absent from the shallow continental shelves, in marked contrast to the extensive deposits found in epeiric basins and on continental margins and shelves in the past. The

challenge for understanding marine black shale distribution, thickness and - importantly - internal variations in deep time is to better constrain the processes that controlled the location and variability of OC production and burial, and their relationship with atmospheric circulation, ocean currents and dynamic depositional conditions.

[3] There is a general consensus that in shallow marine settings OC accumulated in oxygen-deficient water beneath a stratified water column and resulted from a complex interplay between productivity, preservation and dilution [e.g., *Tyson, 2001*]. The relative contribution of each of these factors is debated but each is directly or indirectly linked to atmospheric circulation, through nutrient supply via fluctuations in continental weathering intensity, precipitation and runoff, wind-driven oceanic upwelling, and large scale surface current systems [*Arthur and Sageman*, 1994]. A comprehensive assessment of the processes and feedbacks operating at $<10^6$ yrs based on sediment data, is difficult and requires both climate simulations and consistent high resolution geologic data from multiple locations [*Wagner et al*., 2013].

[4] Previous research has proposed that the British sector of the Late Jurassic Boreal Seaway, which connected the Tethys Ocean with the proto-Arctic (Figure 1), was governed by subtropical climate conditions [*Sellwood and Valdes*, 2008]. Dry subtropical climate is determined by the position of the pole-ward/descending limb of the atmospheric Hadley Cells, which for paleoclimates can only be constrained indirectly in the geological record through precipitation proxies. Further information on the principles of Hadley Cell dynamics for the present day can be found in [*Yin*, 2005] and for the Mesozoic greenhouse climate in *Wagner et al*. [2013]. Studies for the Cretaceous (highlighted below) provide some general insight on the dominant processes and feedbacks under the paleo-Hadley Cells during global greenhouse conditions that may well also have operated in the Jurassic, and during other time periods of global warmth:

1. Paleogeography affected the global large-scale atmospheric and marine circulation via modulations (strength and position) of the Hadley-Walker circulation and this affected regional precipitation [*Ohba and Ueda*, 2010].
2. Lower latitudinal temperature gradients and poleward expansion of the Hadley Cells, with the descending, subtropical limbs located at around 25–30° [*Hay et al*., 2013].
3. Large latitudinal net moisture changes associated with an intensification of Hadley Cell circulation [*Manabe and Bryan*, 1985].
4. A more vigorous terrestrial hydrological cycle leading to an increased nutrient flux to the oceans with implications for marine productivity and enhanced OC burial [*Hofmann and Wagner*, 2011].

[5] The link between black shale formation and climate are long established [e.g., *Jenkyns*, 1980] and numerous studies have refined these connections and feedbacks and their biogeochemical consequences, particularly in open ocean basins [e.g., *Wagner et al*., 2013] and within the context of short-term global warming [*Jenkyns*, 2003]. It has been shown that seasonal to orbital-scale fluctuations in runoff, upwelling, productivity and seawater redox can translate into black shales as millimeter to meter-scale variations in OC content and quality [e.g., *Kuhnt et al.*, 2005; *Wagner et al.*, 2013], often linked with fluctuations in grain size and mineralogy [*Berger et al*., 1984]. These meter and sub-meter heterogeneities in shale can therefore be used to trace climate patterns during times of deposition and test for the links between orbitally-modulated climate and OC deposition in the past.

[6] Following the conceptual model developed for the subtropical-tropical Cretaceous Atlantic [*Wagner et al*., 2013] the strongest contrasts in depositional conditions and geochemical properties, driven by orbitally-paced wet/dry climate variations, occur beneath the ascending and descending limbs of the Hadley Cell. Beneath the ascending limb, the

101 forcing of nutrient flux via upwelling and monsoonal continental runoff is strongest,
102 producing cycles of highly variable organic matter quantity and quality in the sedimentary
103 record. Beneath the descending limb the influence of trade wind forcing, produces continuous
104 and generally enhanced OM quantity and quality [*Wagner et al*., 2013]. The specific response
105 of the Jurassic Hadley Cell circulation to variable intensities and frequencies of orbital
106 forcing and its impacts on deposition in epeiric basins, particularly at the regional scale, has
107 not yet been tested on core material, defining the scope of this study on the Kimmeridge Clay
108 Formation (KCF), primarily using high resolution data from sections in Dorset and
109 Yorkshire, UK.

110 [7] Our new climate simulations using the HadCM3L model with a paleogeography of
111 the Late Jurassic (155.5 Ma, *Getech*, 2013) indicate warm and wet tropical-like conditions
112 between 35^{o} and 54^{o}N during Boreal summer (June-Sept) in the British sector of the KCF,
113 previously described as 'subtropical' [*Sellwood and Valdes, 2008*]. Our model is consistent
114 with published high resolution climate proxy data from the British sector of the KCF
115 [*Desprairies et al.*, 1995; *Morgans-Bell et al.*, 2001; *Hesselbo et al.*, 2009; *Huang et al.*,
116 2010] that confirm a low latitude climate control on OC productivity and deposition. We
117 therefore expand the Cretaceous concept that at orbital time-scales black shale deposition was
118 directly linked to variation in rainfall intensity associated with the Hadley circulation
119 [*Hofmann and Wagner*, 2011; *Wagner et al.*, 2013] to the Boreal Seaway of the Late Jurassic.
120 If confirmed, this has fundamental implications for the climate and depositional controls and
121 OC burial further north, into the proto-Arctic.

122 2. **Geological setting**

123 [8] Deposition of the KCF occurred during overall global greenhouse conditions with
124 pCO_2 values at least four times higher than present atmospheric levels [*Sellwood and Valdes*,
125 2008]. Consistent with this global climate state, there is no direct geologic evidence for polar

ice sheets at that time [*Dera et al*., 2011]. There is a consensus that the KCF in the Wessex Basin of the UK was deposited in a shelf environment below fair-weather wave base but close to storm wave base [*Macquaker and Gawthorpe*, 1993]. Increasing organic (OC) content of the shales has been used as evidence for transgression during the lower part of the formation [see *Morgans-Bell et al*., 2001]. Fluctuations in water column stratification and bottom water redox are indicated by sedimentology, ichnology and paleontology [*Wignall*, 1989; *Oschmann*, 1991], bulk organic and inorganic geochemistry [e.g., *Tyson et al*., 1979], and biomarkers [*Sælen et al*., 2000]. These independent lines of evidence support highly variable seawater redox conditions, from fully oxic to anoxic and euxinic. The presence of isorenieratene and its derivatives in samples from the *wheatleyensis* to *pectinatus* biozones indicate that the base of the photic zone was periodically euxinic [*Van Kaam-Peters et al*., 1998].

3. **Methods**

[9] The model simulations are run with the HadCM3L model, using the same configuration and spinup procedure as in [*Lunt et al. 2016*]. The model is run for a total of 1422 years, with a CO_2 concentration of 1120ppmv, and a paleogeography of the Late Jurassic (155.5 Ma) including a sea-level highstand line and topography defined using the methods of [*Markwick and Valdes*, 2004]. The final 30 years of the simulation are averaged to provide the climatologies. From these climatologies, we use an automated procedure to identify the ITCZ, adapted from [*Berry and Reeder*, 2014]. Two methods of identification are used; the first is based on the maximum tropical precipitation (blue lines in Appendix Figure A2), which identifies the ITCZ from its surface precipitation expression, and the second on the maximum mid-tropospheric (500mbar) vertical velocity (red lines in Appendix Figure A2), which is a more dynamical definition based on the rapid ascent of buoyant air masses. We also identify subtropical zones using similar precipitation and vertical velocity metrics

151 (black and orange lines in Appendix Figure A2). The automatically located ITCZ and
152 subtropics for the Late Jurassic using the same identification method applied to modern
153 conditions are shown in Appendix Figure A1. Based on these, and the precipitation maps
154 themselves, we define the location of the ITCZ for the Late Jurassic in Figure 2 (red line).
155 We also identify global monsoonal regions during the Late Jurassic (Figure 3a) defined
156 using the criteria of *Wang et al*. [2011] which uses the local summer minus winter
157 precipitation rate that exceeds 2mm/day with local summer precipitation also exceeding 55%
158 of the annual total. Furthermore, we diagnose the modelled Jurassic large-scale atmospheric
159 circulation, including Hadley cells, in terms of cross sections of the vertical and zonal wind
160 speeds (Figure 3b, c).
161 It is important to evaluate how well the model simulates the modern atmospheric
162 circulation relative to observations. Our HadCM3L Pre-Industrial simulation reproduces
163 (Figure3d) the spatial extent of the global monsoon regions from CPC Merged Analysis of
164 Precipitation (CMAP; averaging period: 1979-2011) observations (Figure 3g) to a good
165 degree, Further more we test how well the model reproduces the large-scale circulation
166 (vertical velocity (Figure 3e) and Zonal U-wind (Figure 3f) latitudinal cross-sections)
167 between 169°W-7.5°E (the longitudinal extent of the modern-day UK) against NCEP-
168 Reanalysis v.2 (averaging period: 1979-2014; vertical velocity (Figure 3h) and Zonal U-wind
169 (Figure 3i), latitudinal cross-sections); again the model reproduces the main features to a
170 good degree.
171 [10] Linear sedimentation rates (LSR) and mass accumulation rates (MAR) of OC and
172 bulk shale were calculated for each individual sedimentary cycle as defined by *Kuhnt et al.*
173 [2005], assuming that: (1) LSRs were linear within each sedimentary cycle and that, (2) each
174 of them represents one short eccentricity cycle of 400 kyr (Figure 4). The first assumption
175 may well bear some inaccuracy in respect of short term fluctuations in sedimentation and

winnowing, however we have no further evidence to improve this generalisation. The second assumption is based on spectral analysis of %TOC [*Huang et al.* 2010]. To calculate bulk MARs dry bulk density (DBD) was used following MAR_{bulk} = LSR*DBD with DBD obtained from the literature [*Leine*, 1986; *Kuhnt et al*., 1997]. %TOC values are corrected for carbonate content using the following: TOC carbonate-free % = 100/(100-carbonate %)*%TOC. The relationship between kaolinite/illite ratio and %TOC carbonate-free is based on data from Dorset [www.earth.ox.ac.uk/~rgge/data.html].

4. **Results**

4.1 **Climate simulations**

[11] Figures 2 and 3 (and Appendix Figures A1, A2) show the ITCZ as identified using the two criteria defined in the methods section. Contrary to the modern situation (for reference also shown in Appendix), in June/July/August (JJA) the ITCZ splits as it reaches the American continent from the east Pacific, resulting in a northern arm, which is pinned by the proto-Appalachian mountain range, and a southern arm, which is pinned by the North African mountain range. Of these, the northern arm is strongest, and extends to about 30^{o}N in the region of the KCF of the UK. Figure 3 further supports the positon of this northward propagation of the ITCZ shown by the maximum northward extension of the N.H. Hadley-circulation (~35°N in August) with weak (relative to the simulated Pre-Industrial (3e) and Modern-day (3h)) vertical motion. The northward extension of the Hadley Cell is associated with a >15° northward migration in the sub-tropical jet from ~35-40°N in June to ~55-60°N in August (Figure 3c). This rapid northward movement in the sub-tropical jet does have a modern-day analogue in being a key process that initializes the Indian monsoon system. With the boreal seaway region in the simulation also being shown to be monsoonal (Figure 3a) we

200 can surmise that both a northward extension of the ITCZ and monsoonal conditions in the
201 model will have an influence on the depositional environment.
202 Moving eastwards, the ITCZ is then deflected southwards into the tropical Tethys Ocean.
203 Notably, the area of enhanced humidity is also pulled north on both sides of the NW
204 European Boreal Seaway up to the Arctic Ocean, driven by elevated regions along the
205 coastlines of Canada and Scandinavia. The character of the Indian and East Asian monsoons
206 in the modelled Kimmeridgian had less continental precipitation compared to the modern. As
207 for the modern, in December/January/February (DJF), the ITCZ is in the Southern
208 Hemisphere, but the Jurassic ITCZ does not deflect as strongly over South America or Africa.
209 Figure 2 (and Appendix Figures A1 and A2) also show the location of the dry subtropical-like
210 regions between 45^{o} and 60^{o}N, with the associated descending arm of the Hadley Cell shown
211 by the green line in Figure 3c. This broadly parallels the ITCZ in the northern hemisphere. It
212 extends across Laurentia into the paleo-Arctic Ocean in the vicinity of the Boreal Seaway and
213 southwards into central Europe-Asia. At least between 5.625-24.375°E longitudes and
214 consistent with the sub-tropical jet core being centred around 55-60°N (Figure 3c).
215 4.2 **Sedimentology, depositional environment and astrochronolgy**
216 [12] Much of the Kimmeridge Clay Formation has a high OC content, but the most
217 enriched interval occurs in the *wheatleyensis–hudlestoni* zones, where TOC frequently
218 exceeds 10% [*Tyson*, 1996] (Figure 4). The depositional and preservational conditions during
219 these specific periods are therefore of particular interest.
220 [13] The three lithologies common to much of the formation – grey shale, black shale, and
221 coccolith limestone – are present in the *wheatleyensis–hudlestoni* zones, suggesting that the
222 depositional conditions were broadly similar to those interpreted elsewhere in the succession.
223 The grey shales of the upper *wheatleyensis* Zone are homogenized. This homogenisation
224 could have resulted from physical or biogenic (bioturbation) processes, or a combination of

the two. In the Clavell's Hard Stone Band, for example occasional *Planolites* trace fossils are seen in homogeneous grey mudstone (Figure 5e), providing evidence that the sediment was being intensely processed by infauna.

[14] The succession above the Clavell's Hard Stone Band becomes increasingly OC-rich, with a transition from grey shales to extremely OC-rich black shales (>20% TOC) just below the Blackstone Band. The sedimentology is distinctive, with the black shales being formed of thin, event beds, with a somewhat 'lenticular' fabric (Figures 5a, 5d). These lenses might be compressed ripples, bedding-parallel trace fossils, or ripped-up clasts of (microbially bound?) mud, possibly both. Burrow diameters (often >5 mm) indicates that energetic and probably oxic conditions were present at the sediment-water interface; silty, bioclastic mudstones (Figure 5b) and low-angle ripple cross-bedding (Figure 5i) also provide support for dynamic seafloor processes.

[15] Above the Blackstone Band the %TOC remains high, but the lithology changes again, with the lower *hudlestoni* Zone being marked by increasing quantities of primary carbonate from coccoliths (Figure 5c). The Rope Lake Head Stone Band and White Stone Band are coccolith limestones (Figures 5f, 5g, 5h), rather than the dolomitic stone bands of the type present lower in the succession. The Rope Lake Head is also noticeable in containing the first large, ichnofabric-forming trace fossils: a low diversity ichnofauna dominated by faecal pellet-rich specimens of *Rhizocorallium* (Figure 5f). Burrows of this size [shaft diameter >10 mm] strongly support oxic conditions at the sediment-water interface, at least periodically, and are also seen in the White Stone Band (Figure 5h). The low diversity of trace makers, however, suggests that other restricting factors were present. The occurrence of grey shales homogenized by small infauna, black shales deposited as event beds, and OC-rich coccolith limestones colonized by specialized deposit-feeders is indicative of a more dynamic dysoxic–oxic environment. Our observations are consistent with those of *Wignall* [1991] who

reported the upper dysaerobic biofacies contained a moderately diverse, un-tiered assemblage with *Rhizocorallium* and *Chrondrites,* developed in a surface mixed layer.

[16] Figure 6 shows a stratigraphical cross plot between "basin-centered" sections in Dorset and Yorkshire and the more proximal, shoreface section at Boulonnais, northern France. Notably, high resolution correlations of individual %TOC peaks can confidently be made between Dorset and Yorkshire, over a distance of ~400 km, they cannot be made to the Boulonnais section in northern France.

[17] A multi-proxy record with a pronounced cyclicity has been obtained from the Swanworth and Metherhills cores from the Wessex Basin [*Weedon et al*., 2004]. These records were further refined and tuned to the 405-kyr and 100-kyr eccentricity signals [*Huang et al*., 2010]. *Huang et al.* [2010] identified a hierarchy of cycles in both un-tuned and tuned (at 405-kyr) %TOC and Formation Micro-Scanner (FMS) data throughout the formation. Their analysis showed the ~2 Myr (~167 m), ~405-Kyr (~40 m) and ~100-Kyr (9–18m) eccentricity; ~40-Kyr obliquity (2.3–4.8 m) and ~20-Kyr precession (1.25–1.62 m) cycles.

4.3 **Linear sedimentation**

[18] On average, LSRs are high, on the order of about 6 cm/kyr to 11 cm/kyr (Figure 4). The general pattern indicates the presence of a lower but irregular frequency rhythm being superimposed on the well-developed bed-set cycles. This rhythm is independent of the other parameters and therefore attributable to local factors including topography, bottom water currents, storm activity and sediment grain size.

4.4 **Mass accumulation rates**

[19] Organic matter in the KCF is dominated by Type II marine amorphous kerogen with minor Type I and III [*Farrimond et al.*, 1984; *Scotchman*, 1991]. Type III kerogen, though generally rare, is most abundant in basin margin settings, whilst Type II kerogens were

restricted to basin centres. Hydrogen indices vary between ~120 and 550 mgHC/gTOC [*Tyson*, 2004] and are lower in proximity to the inferred paleo-shoreline and higher in more distal settings [*Scotchman*, 1991]. The section containing the highest %TOC is characterised by a positive $\delta^{13}C_{org}$ excursion that spans the *eudoxus* to mid-*hudlestoni* zones. This interval has an average >5 wt% TOC [*Morgans-Bell et al.*, 2001] (Figure 4).

[20] OC burial and %TOC carbonate-free are both high for the Kimmeridge section and show similar patterns (Figure 4). Both increase from low values from the base of the section up to the middle of the *huddlestoni* Zone. They fall back within the lower *huddlestoni* Zone but then rise to through the remaing *huddlestoni* to mid-*pectinatus* Zone. Above this, there is a gradual decline back to low values at the top of the section. Superimposed on the long-term trend are distinct higher-frequency and high-amplitude fluctuations both parameters (Figure 4). Fluctuations in TOC are observed on ~40 m to sub-millimeter long cycle scales. These amplitudes are generally higher from the *eudoxus* to mid-*huddlestoni* zones.

[21] For much of the record, periods of maximum OC burial and kaolinite/illite ratio are structured into bundles of four peaks per 400-kyr cycle (Figure 7). Based on the age model for the KCF this suggests an assigned frequency of 100-kyr for each of these peaks and therefore these likely reflect short eccentricity fluctuations in climate and OC MAR. Higher frequency fluctuations at the obliquity and precessional orbital bands are not resolved in the proxy records.

4.5 **Continental climate**

[22] In addition to the orbital scale fluctuations there are clear longer term trends in the kaolinite/illite record from the Dorset section [*Hesselbo et al.*, 2009] (Figures 4, 7). The record shows an increase in the ratio from 1 in the *cymodoce* Zone to a peak of 2.6 in the

299 mid-*autissiodorensis* Zone. This is followed by a decline back to a value of 1 at the top of the
300 *huddlestoni* Zone and a further rise to 2 in the *rotunda* Zone.

301 5. **Discussion**

302 [23] Our new climate simulations indicate a poleward shift to around ~35-40°N of high
303 precipitation tropical-like regions, associated with changes in the Hadley circulation during
304 the Late Jurassic greenhouse, likely driven by the clustered distribution of land masses
305 surrounding the proto North Atlantic and western Tethys region and topographic effects from
306 mountain ranges along the coastlines of North America and North Africa, and along the
307 Boreal Seaway. This climate scenario would be consistent with storm-influenced
308 sedimentation via intensification of tropical storm tracks in a shallow water setting.
309 Sedimentary textures indeed indicate that storms had a significant influence on sedimentation
310 during the most OC-rich parts of the KCF. This is consistent with a variety of storm-produced
311 event beds described from the KCF, including horizons of graded rip-up clasts, silt laminae,
312 thin graded mud horizons and shell pavements [*Wignall*, 1989]. A mechanism of storm-
313 induced benthic oxygenation and temperature-stratified inhibition of storm mixing has been
314 proposed for the abrupt nature of the decimeter-scale organic-rich and organic-lean shales in
315 the KCF [*Wignall*, 1989].

316 [24] The kaolinite/illite ratio is a well-established proxy for continental climate and
317 associated land surface processes. Kaolinite commonly forms in soils under tropical humid
318 conditions [*Thiry*, 2000]. In shelf basins, where riverine input of clay minerals is highest and
319 often rapid, lateral transport of the mineral load occurs primarily with strong surface currents
320 and during storm events, preserving an almost direct record of continental climate [*Singer*,
321 1984]. An alternative, diagenetic origin for the kaolinite in the KCF has been rejected based
322 on petrography and regional considerations [*Hesselbo et al*., 2009]. Burial maturation in the
323 Kimmeridge Clay is also compatible with the occurrence of smectite which is only rarely

deposited in the Wessex and Cleveland basins [*Hesselbo et al*., 2009]. Figure 7 shows the relationship between kaolinite/illite ratio and %TOC carbonate-free records as indicators of wet/dry conditions and OC burial respectively. Superimposed on the long-term (million year) trend are distinct higher-frequency and high-amplitude fluctuations at ~40m and ~10m-scale. These high-amplitude and short-term variations occurred synchronously for TOC carbonate-free (and %TOC) and kaolinite/illite ratio on a sample-by-sample basis. Based on a mean LSR of 8.25 cm/ka these equate with the 405-kyr and 100-kyr eccentricity cycles.

[25] The consistency of this variability in OC MAR and kaolinite/illite ratio in these orbital power bands strongly supports a close link to climate forcing. Sedimentation, as indicated by bulk accumulation and carbonate accumulation rates in the British sector during the KCF, however, did not react in a strictly uniform manner to these orbital climate variations which we attribute to local effects of topography, currents, sediment grain size, and/or productivity.

[26] %TOC peak to peak correlation between the Swanworth core in Dorset and the Ebberston 87 core in Yorkshire indicate this situation extended over a distance of 400km. The principle mechanisms responsible for these distinct patterns are hypothesized to be variations in marine productivity followed by stratification-driven anoxia. Furthermore, OC burial and black shale formation must have been intimately linked to climate-modulated fluctuations in nutrient cycling. The supply of clay minerals from continental sources suggests continental runoff as a primary mechanism controlling nutrient supply, and thus black shale formation, consistent with organo-mineral studies of Cretaceous open marine OAE black shale sections [*Kennedy and Wagner*, 2011; *Loehr and Kennedy*, 2014].

[27] This conclusion is expected from the geological context, as the close vicinity of the Boreal Seaway to the Euro-American continent and the warm global climate during the late-

348 Jurassic should have stimulated an intensified hydrological cycle with high precipitation and
349 runoff [*Selwood and Valdes 2008*].
350 [28] Orbital-scale variations in OC content are well-known for marine black shales from
351 numerous geological periods. They have been related to: 1) increased OC flux to the seafloor
352 induced by productivity pulses ; 2) climate-induced variations in organic productivity,
353 coupled with variations in bottom water redox [*Sælen et al*., 2000 and references therein], 3)
354 water column stratification [*Tyson et al*., 1979], and 4) climate controlled production of
355 expandable clay minerals (smectite-type) into oxygen depleted continental margin settings,
356 catalysing OC burial via organo-mineral interactions [*Kennedy and Wagner*, 2011].
357 [29] Following the conceptual model for the Cretaceous, enhanced runoff would have
358 promoted the establishment of anoxia/ euxinia and black shale formation along the Boreal
359 Seaway through enhanced marine productivity. Conversely, reduced runoff would have
360 resulted in reduced nutrient flux and marine productivity and thus partial re-establishment of
361 oxic conditions in the water column. As demonstrated by the climate model such a situation
362 would correspond to a more northerly position of the Intertropical Convergence Zone (ITCZ)
363 during the late Jurassic. There is a remarkable consistency between the evidence deduced
364 from the climate modelling and the sedimentological record across the British sector. This
365 leads us to suggest that OC burial and black shale deposition in the KCF was intimately
366 linked to precipitation changes that can be associated with orbital time scale fluctuations in
367 the atmospheric circulation, and in particular changes in the extent of the Hadley Cells.
368 [30] Our alternative interpretation of prevailing climatic conditions in the southern part of
369 the Late Jurassic Boreal Seaway implies a maximum reach of the ITCZ as far north as ~35^{o}N.
370 Such a scenario recognizes the substantially wider latitudinal shift of the ITCZ in the modern
371 Pacific region compared to the Atlantic region, with the ITCZ migrating seasonally over ~60^{o}
372 of latitude and a maximum northern position at ~35^{o}N during Boreal summer. Identification

of the outer subtropical boundary hints towards a low latitude influence on marine sedimentation and OC burial in the Arctic sector of the Boreal Seaway. *Mutterlose et al*., [2003] reported OC-rich Kimmeridgian-Tithonian aged shales as far north as the Barents Sea (54^{o}N in the Late Jurassic), with sedimentary cycles containing a distinct precessional-pacing, consistent with some influence from low latitude fluctuations in insolation. In the late Jurassic the northern Hadley Cell may therefore have extended, at least temporarily, imposing dynamic, subtropical conditions close to the paleo-Arctic.

[31] We therefore propose that orbital forcing in the Late Jurassic would have controlled alternations between extremely humid conditions, supporting peak OC burial in the KCF, and dryer periods where freshwater supply and redox conditions relaxed, resulting in lower OC burial. A depositional system with strongly alternating hydrological conditions is consistent with many black shales from the Cretaceous Oceanic Anoxic Events [*Beckmann et al*., 2005] and the Neogene Mediterranean sapropels [*Rossignol-Strick*, 1985].

[32] The onset of a drier climate in the upper Tithonian of the British sector may indicate a gradual transition to a more subtropical climate with stronger trade winds. The underlying mechanism for this large scale shift in climate conditions remains unclear, but a link to the long-term and global scale drawdown of CO_2 during peak Kimmeridgian black shale deposition has been proposed [see also *Wignall and Ruffell* 1990]. These conditions would have promoted global cooling and eventually incipient glaciation [*Donnadieu et al*., 2011]. The emergence of incipient south polar ice sheets in the later Tithonian should have led to an increase in global surface meridional temperature gradient and a contraction of the outer boundaries of the Hadley Cells, gradually shifting the British KCF out of the direct influence of tropical and eventually also subtropical climate conditions.

6. **Conclusions**

[33] The Kimmerdige black shales from the late Jurassic epeiric Boreal Seaway were deposited at high average sedimentation rates (8 cm/kyr) enabling the investigation of paleoclimate and paleoceanography at high temporal resolution and associated hydrocarbon source-rock formation. The KCF was deposited between ~35^{o}N and ~65^{o}N in temperature- or salinity-stratified sub-basins. Deposition was strongly influenced by frequent storm activity and high rates of sedimentation leading to expanded shale sections and massive burial of organic matter. Analyses of the relationships between clay mineral assemblages (kaolinite/illite) and OC content support the conclusion that changes in OC burial resulted from orbitally-paced fluctuation in rainfall intensity beneath the ascending limb of the Hadley Cell, i.e. under the direct influence of the tropical ITCZ. Our new climate simulations support this tropical scenario. Together these suggest that the variable but overall very high burial of OC in the KCF was controlled by very similar mechanisms as some of the Cretaceous OAE's and the Mediterranean sapropels.

[34] The implications of this re-interpretation of high resolution records from Dorset and Yorkshire for temperate and sub-polar depositional settings in the Late Jurassic are yet unclear. These may have been profound, affecting the location of frontal systems, runoff patterns, salinity stratification, and gradients in sea surface temperature and sea water redox. Additional high resolution records from the northern Boreal Seaway and the proto-Arctic combined with model simulations incorporating orbital variability explicitly are needed to validate and constrain the wider implications of the Jurassic model proposed in this study.

Acknowledgements

Funding was provided by NERC Oil and Gas Catalyst Grant (NE/L008092/1) and the Durham University PVC Research Seedcorn Fund. DJL and AF acknowledge NERC grant NE/K014757/1. We acknowledge fruitful discussions with many colleagues, particularly Dr

J. Trabucho-Alexandre and Dr R.V. Tyson. Lauren Raynham and Amanda Galsworthy from the " Getech Globe" paleogeographic mapping team were essential in producing the basemaps used in this study. The helpful comments of the anonymous referees and editor significantly improved this paper. Supplementary information can be found at …….

References

Arthur, M. A., and B. B. Sageman (1994), Marine black shales: depositional mechanisms and environments of ancient deposits, *Annu. Rev. Earth Planet. Sci.*, *22*, 499-551.

Beckmann, B., T. Wagner, and P. Hofmann (2005), Linking Coniacian-Santonian (OAE3) black shale deposition to African climate variability: a reference section from the eastern tropical Atlantic at orbital timescales (ODP site 959, Off Ivory Coast and Ghana), *SEPM Special Publication*, *82*, 125-143.

Berger, A., J. Imbrie, J. Hays, G. Kukla, and B. Saltzman (1984), *Milankovitch and Climate. Understanding the Response to Orbital Forcing*, Reidel Publishing Company, Amsterdam.

Berry, G., and M. J. Reeder (2014), Objective identification of the intertropical convergence zone: Climatology and trends from the ERA-Interim, *Journal of Climate*, *27*(5), 1894-1909.

Dera, G., B. Brigaud, F. Monna, R. Laffont, E. Pucéat, J.-F. Deconinck, P. Pellenard, M. M. Joachimski, and C. Durlet (2011), Climatic ups and downs in a disturbed Jurassic world, *Geology*, *39*(3), 215-218.

Desprairies, A., M. Bachaoui, A. Ramdani, and N.-P. Tribovillard (1995), Clay diagenesis in organic-rich cycles from the Kimmeridge Clay Formation of Yorshire (G.B.): implication for palaeoclimatic interpretations, in *The Organic Cyclicities of the Kimmeridge Clay Formation (Yorkshire, GB) and the Recent Maar Sediments (Lac du Bouchet, France). Lecture Notes in Earth Sciences*, edited by E. Lallier-Verges, N.-P. Tribovillard and P. Bertrand, pp. 63-91, Springer.

448 Donnadieu, Y., G. Dromart, Y. Goddéris, E. Pucéat, B. Brigaud, G. Dera, C. Dumas, and N.
449 Olivier (2011), A mechanism for brief glacial episodes in the Mesozoic greenhouse,
450 *Paleoceanography*, *26*(3), PA3212.
451 Farrimond, P., P. Comet, G. Eglinton, R. P. Evershed, M. A. Hall, D. W. Park, and A. M.
452 Wardroper (1984), Organic geochemical study of the Upper Kimmeridge Clay of the
453 Dorset type area, *Marine and Petroleum Geology*, *1*(4), 340-354.
454 Getech (2013), Atlases of Global Palaeogeography - Jurassic.
455 Hay, W., R. DeConto, and S. Flögel (2013), Cretaceous continental hydrology–different from
456 today, *Earth-Science Reviews*, *115*(4), 262-272.
457 Herbin, J.-P., C. Muller, J. Geyssant, F. Melieres, and I. Penn (1991), Hétérogénéité
458 quantitative et qualitative de la matiére organique dand les argiles du Kimméridgien du Val
459 de Pickering (Yorkshire, UK): cadre sédimentologique et stratigraphique, *Revue de*
460 *l'Institut français du pétrole*, *46*(6), 675-712.
461 Hesselbo, S. P., J.-F. Deconnick, J. M. Huggett, and H. S. Morgans-Bell (2009), Late Jurassic
462 palaeoclimatic change from clay mineralogy and gamma-ray spectrometry of the
463 Kimmeridge Clay, Dorset, UK, *Journal of the Geological Society*, *166*(6), 1123-1133.
464 Hofmann, P., and T. Wagner (2011), ITCZ controls on Late Cretaceous black shale
465 sedimentation in the tropical Atlantic Ocean, *Paleoceanography*, *26*(4), PA002154.
466 Huang, C., S. P. Hesselbo, and L. Hinnov (2010), Astrochronology of the late Jurassic
467 Kimmeridge Clay (Dorset, England) and implications for Earth system processes, *Earth*
468 *and Planetary Science Letters*, *289*(1–2), 242-255.
469 Jenkyns, H. C. (1980), Cretaceous anoxic events: from continents to oceans, *Journal of the*
470 *Geological Society*, *137*, 171-188.

471 Jenkyns, H. C. (2003), Evidence for rapid climate change in the Mesozoic–Palaeogene
472 greenhouse world, *Philosophical Transactions of the Royal Society of London. Series A:*
473 *Mathematical, Physical and Engineering Sciences*, *361*(1810), 1885-1916.
474 Kennedy, M. J., and T. Wagner (2011), Clay mineral continental amplifier for marine carbon
475 sequestration in a greenhouse ocean, *Proceedings of the National Academy of Sciences*,
476 *108*(24), 9776-9781.
477 Kuhnt, W., F. Luderer, S. Nederbragt, J. Thurow, and T. Wagner (2005), Orbital-scale record
478 of the late Cenomanian–Turonian oceanic anoxic event (OAE-2) in the Tarfaya Basin
479 (Morocco), *International Journal of Earth Sciences*, *94*(1), 147-159.
480 Löhr, S. C., and M. J. Kennedy (2014), Organomineral nanocomposite carbon burial during
481 Oceanic Anoxic Event 2, *Biogeosciences*, *11*, 4971-4983.
482 Lunt, D. J., A. Farnsworth, C. Loptson, G. L. Foster, P. Markwick, C. L. O'Brien, R. D.
483 Pancost, S. A. Robinson, and N. Wrobel (2016, *in press*), Palaeogeographic controls on
484 climate and proxy interpretation, *Climate Past*.
485 Macquaker, J., and R. Gawthorpe (1993), Mudstone lithofacies in the Kimmeridge Clay
486 Formation, Wessex Basin, southern England: implications for the origin and controls of
487 the distribution of mudstones, *Journal of Sedimentary Research*, *63*(6), 1129-1143.
488 Manabe, S., and K. Bryan (1985), CO_2-induced change in a coupled ocean-atmosphere model
489 and its paleoclimatic implications, *Journal of Geophysical Research: Oceans (1978–*
490 *2012)*, *90*(C6), 11689-11707.
491 Markwick, P. J., and P. J. Valdes (2004), Palaeo-digital elevation models for use as boundary
492 conditions in coupled ocean–atmosphere GCM experiments: a Maastrichtian (late
493 Cretaceous) example, *Palaeogeography, Palaeoclimatology, Palaeoecology*, *213*(1), 37-
494 63.

Morgans-Bell, H. S., A. L. Coe, S. P. Hesselbo, H. C. Jenkyns, G. P. Weedon, J. E. A. Marshall, R. V. Tyson, and C. J. Williams (2001), Intergrated stratigraphy of the Kimmerdige Clay Formation (Upper Jurassic) based on exposures and boreholes in south Dorset, UK, *Geological Magazine*, *138*, 511-539.

Mutterlose, J., H. Brumsack, S. Flögel, W. Hay, C. Klein, U. Langrock, M. Lipinski, W. Ricken, E. Söding, and R. Stein (2003), The Greenland-Norwegian Seaway: A key area for understanding Late Jurassic to Early Cretaceous paleoenvironments, *Paleoceanography 18*(1), PA000625.

Ohba, M., and H. Ueda (2010), A GCM study on effects of continental drift on tropical climate at the early and late Cretaceous, *Journal of the Meteorological Society of Japan*, *88*(6), 869-881.

Oschmann, W. (1991), Distribution, dynamics and palaeoecology of Kimmeridgian (Upper Jurassic) shelf anoxia in western Europe, in *Modern and ancient continental shelf anoxia*, edited by R. V. Tyson and T. H. Pearson, pp. 381-395, Geological Society of London. Special Publication.

Rossignol-Strick, M. (1985), Mediterranean Quaternary sapropels, an immediate response of the African monsoon to variation of insolation, *Palaeogeography, Palaeoclimatology, Palaeoecology*, *49*(3), 237-263.

Sælen, G., R. Tyson, N. Telnæs, and M. Talbot (2000), Contrasting watermass conditions during deposition of the Whitby Mudstone (Lower Jurassic) and Kimmeridge Clay (Upper Jurassic) formations, UK, *Palaeogeography, Palaeoclimatology, Palaeoecology*, *163*(3), 163-196.

Scotchman, I. C. (1991), Kerogen facies and maturity of the Kimmeridge Clay Formation in southern and eastern England, *Marine and Petroleum Geology*, *8*, 278-295.

519 Sellwood, B. W., and P. J. Valdes (2008), Jurassic climates, *Proceedings of the Geologists'*
520 *Association*, *119*(1), 5-17.
521 Singer, A. (1984), The paleoclimatic interpretation of clay minerals in sediments—a review,
522 *Earth-Science Reviews*, *21*(4), 251-293.
523 Thiry, M. (2000), Palaeoclimatic interpretation of clay minerals in marine deposits: an
524 outlook from the continental origin, *Earth-Science Reviews*, *49*(1), 201-221.
525 Tribvollard, N., T. J. Algeo, T. W. Lyons, and A. Riboulleau (2006), Trace metals as
526 paleoredox and paleoproductivity proxies: an update, *Chemical Geology*, *232*, 12-32.
527 Tyson, R. V. (1996), Sequence-stratigraphical interpretation of organic facies variations in
528 marine siliciclastic systems: general principles and application to the onshore Kimmeridge
529 Clay Formation, UK., in *Sequence stratigraphy in British Geology*, edited by S. P.
530 Hesselbo and D. N. Parkinson, pp. 75-96, Geological Society, London, Special Publication
531 103.
532 Tyson, R. (2001), Sedimentation rate, dilution, preservation and total organic carbon: some
533 results of a modelling study, *Organic Geochemistry*, *32*(2), 333-339.
534 Tyson, R. V. (2004), Variation in marine total organic carbon through the type Kimmeridge
535 Clay Formation (Late Jurassic), Dorset, UK, *Journal of the Geological Society*, *161*(4),
536 667-673.
537 Tyson, R. V., R. C. L. Wilson, and C. Downie (1979), A stratified water column model for the
538 type Kimmeridge Clay, *Nature*, *277*, 377-380.
539 Van Kaam-Peters, H. M., S. Schouten, J. Köster, and J. S. S. Damstè (1998), Controls on the
540 molecular and carbon isotopic composition of organic matter deposited in a Kimmeridgian
541 euxinic shelf sea: Evidence for preservation of carbohydrates through sulfurisation,
542 *Geochimica et Cosmochimica Acta*, *62*(19), 3259-3283.

Wagner, T., P. Hofmann, and S. Flögel (2013), Marine black shale deposition and Hadley Cell dynamics: A conceptual framework for the Cretaceous Atlantic Ocean, *Marine and Petroleum Geology*, *43*(0), 222-238.

Wang, W., P. Xie, S.-H. Yoo, Y. Xue, A. Kumar, and X. Wu (2011), An assessment of the surface climate in the NCEP climate forecast system reanalysis, *Climate Dynamics*, *37*(7-8), 1601-1620.

Weedon, G. P., A. L. Coe, and R. W. Gallois (2004), Cyclostratigraphy, orbital tuning and inferred productivity for the type Kimmeridge Clay (Late Jurassic), Southern England, *Journal of the Geological Society*, *161*, 655-666.

Wignall, P. B. (1989), Sedimentary dynamics of the Kimmeridge Clay: tempests and earthquakes, *Journal of the Geological Society*, *146*(2), 273-284.

Wignall, P. B. (1991), Dysaerobic Trace Fossils and Ichnofabrics in the Upper Jurassic Kimmeridge Clay of Southern England, *Palaios*, *6*(3), 264-270.

Wignall, P. B., and A. H. Ruffell (1990), The influence of a sudden climatic change on marine deposition in the Kimmeridgian of northwest Europe, *Journal of the Geological Society*, *147*(2), 365-371.

Yin, J. H. (2005), A consistent poleward shift of the storm tracks in simulations of 21st century climate, *Geophysical Research Letters*, *32*(18).

Figure captions

Figure 1. Paleogeography of NW Europe for the Kimmeridgian Stage (provided by Getech Group plc) including the sea-level highstand line and the Present Day countries rotated to their palaeopositions. The distribution of the Hadley Cell and associated climate belts is based on previous work (*Sellwood and Valdes* [2008]), which we revise in this paper.

Figure 2. Modelled precipitation (contours, mm/day), location of the Intertropical Convergence Zone (ITCZ, red line) during the deposition of the KCF based on HadCM3L model and a paleogeography of the Late Jurassic [155.5 Ma, *Getech*, 2013]. Upper map is boreal summer (June, July, August), and lower map is boreal winter (December, January, February). During Boreal summer the ITCZ lies in a more northerly location than at the present day placing the Boreal sector of the NW European seaway temporarily under tropical-like conditions. The green line shows the approximate 1mm/day precipitation contour, whose position is influenced by the location of the descending limb of the Hadley Cell and the subtropical jet, as indicated in Figure 3b, c.

Figure 3. Global monsoon regions (highlighted in green) as defined by *Wang et al*. [2012] during the Late Jurassic (Kimmeridgian) simulation (a), Pre-industrial simulation (d) and for CMAP observations (g) with topography shaded in grey. Latitudinal vertical velocity cross-section for paleo-UK (Kimmeridgian: 32.4°N, 15.3°E +/-10° mean; Modern: 1W°, 52°N) in the Kimmeridgian simulation (b), Pre-Industrial simulation (e; (longitudinal mean 168.75°W-7.5°E) and NCEP-Reanalysis v.2 (h; longitudinal mean 168.75°W-7.5°E) indicates the maximum extent of the Hadley-circulation where each coincides during August. Vertical ascent is denoted by negative values while positive values denote descent. Latitudinal zonal U-wind cross-section for paleo-UK (Kimmeridgian: 32.4°N, 15.3°E +/-10° mean; (Modern: 1W°, 52°N)) in the Kimmeridgian simulation (b), Pre-Industrial simulation (f; (longitudinal mean 168.75°W-7.5°E) and NCEP-Reanalysis v.2 (i; longitudinal mean 168.75°W-7.5°E) indicates zonal westerlies (positive values) and zonal easterlies (negative values). Black vertical lines depict the latitudinal extent of the modern UK and paleo-rotated UK in the Kimmeridgian.

Figure 4. Conflated records of key sedimentological, climate and organic carbon burial proxy data from the Kimmeridge Clay Formation in Dorset. Chronostratigraphy, lithostratigraphy,

591 $\delta^{13}C_{org}$, %TOC are after *Morgans-Bell et al.* [2001]; clay mineral data are from [*Hesselbo et*
592 *al*., 2009]. Stone Bands: BB2, Blake's Bed 2; FWS, Fresh Water Steps; WSB, White Stone
593 Band; BaSB, Basalt; SJC, Short Joint Coal; RLH, Rope Lake head; BSB, Blackstone Band;
594 CHSB, Clavell's Hard; GLSB, Grey Ledge; CLSB, Cattle Ledge; YL, Yellow Ledge; Bb42,
595 Blake's Bed 42; MLSB, Maple Ledge; WLSB, Washing Ledge; TFSB, The Flats; MSB,
596 Metherhills.

597 **Figure 5**. Sedimentary textures from the Kimmeridge Clay Formation, Kimmeridge, UK. (a)
598 Laminated black shale; scale bar: 10 mm. (b) ESEM image of silty, bioclastic mudstone;
599 scale bar: 80 μm. (c). Laminated, organic-rich shale and coccolith limestone; Freshwater
600 Steps Stone Band; Swanworth Quarry borehole. (d) Fractured silty grey mudstone, 119m
601 depth (upper *eudoxus* Zone), Metherhills borehole; scale bar: 10 mm. (e) Homogeneous
602 (bioturbated) grey mudstone with *Planolites* (Pla) trace fossil, Clavell's Hard Stone Band
603 (mid-*wheatleyensis* Zone); scale bar: 10 mm. (f) *Rhizocorallium* (Rhz) trace fossil in
604 homogenized coccolith limestone, burrow showing spreiten formed of organic matter-rich
605 faecal pellets; Rope Lake Head Stone Band (lower *hudlestoni* Zone); hand lens: 50 mm. (g)
606 ESEM image of coccolith limestone, White Stone Band (lower *pectinatus* Zone); scale bar:
607 20 μm. (h) *Rhizocorallium* (Rhz)-dominated ichnofabric in coccolith limestones and black
608 shales of White Stone Band (lower *pectinatus* Zone). Note coccolith-rich spreiten in lower
609 specimen; organic-mud rich spreiten in upper specimen; scale bar: 10 mm. (i) Cross-
610 laminated, organic-rich mudstones, 257.3 m depth (*wheatleyensis* Zone), Swanworth Quarry
611 borehole; scale bar: 10 mm.

612

613 **Figure 6**. Stratigraphical cross-plot of the type Kimmeridge Clay in Dorset [*Morgans-Bell et*
614 *al.*, 2001], Yorkshire (right: Ebberston 87 core after *Herbin et al*. [1991]) and Boulonnais
615 (left; Créche section, redrawn after *Tribvollard et al*. [2006]). Creche section is simplified to

616 black, shales and the white boxes are shoreface sandstones. Stratigraphical scales are in
617 metres. Organic-rich intervals (ORI 1-5) as defined by *Herbin et al*. [1991].
618
619 **Figure 7**. Relationship between kaolinite/illite and %TOC carbonate-free over depth. 400-kyr
620 cycles are as defined by *Huang et al.* [*2010*].

11°15'W 3°45'W 0° 3°45'E 11°15'E 18°45'E 26°15'E 33°45'E 41°15'E

62°30'N 57°30'N 52°30'N 47°30'N 42°30'N 37°30'N 32°30'N 27°30'N

Ba

C

K

B

As proposed by Sellwood & Valdes (2008)

Ferrell Cell

Temperate

?

?

Outer Hadley Cell

Subtropical

Land

K Kimmeridge-Wessex Basin

C Cleveland Basin

B Boulonnais

Ba Barents Sea

60° N
30° N
0°
30° S
60° S
60° N
30° N
0°
30° S
60° S
60° N
30° N
0°
30° S
60° S
60° N
30° N
0°
30° S
60° S

Legend

Kimmeridgian Highstand
ITCZ

Lithology

Volcanics
Igneous Intrusives
Evaporites
Carbonates
Fine Clastics
Coarse Clastics

Precipitation mm/day

0 - 0.5
0.5 - 1
1 - 2
2 - 4
4 - 8
8 - 16
16 - 32

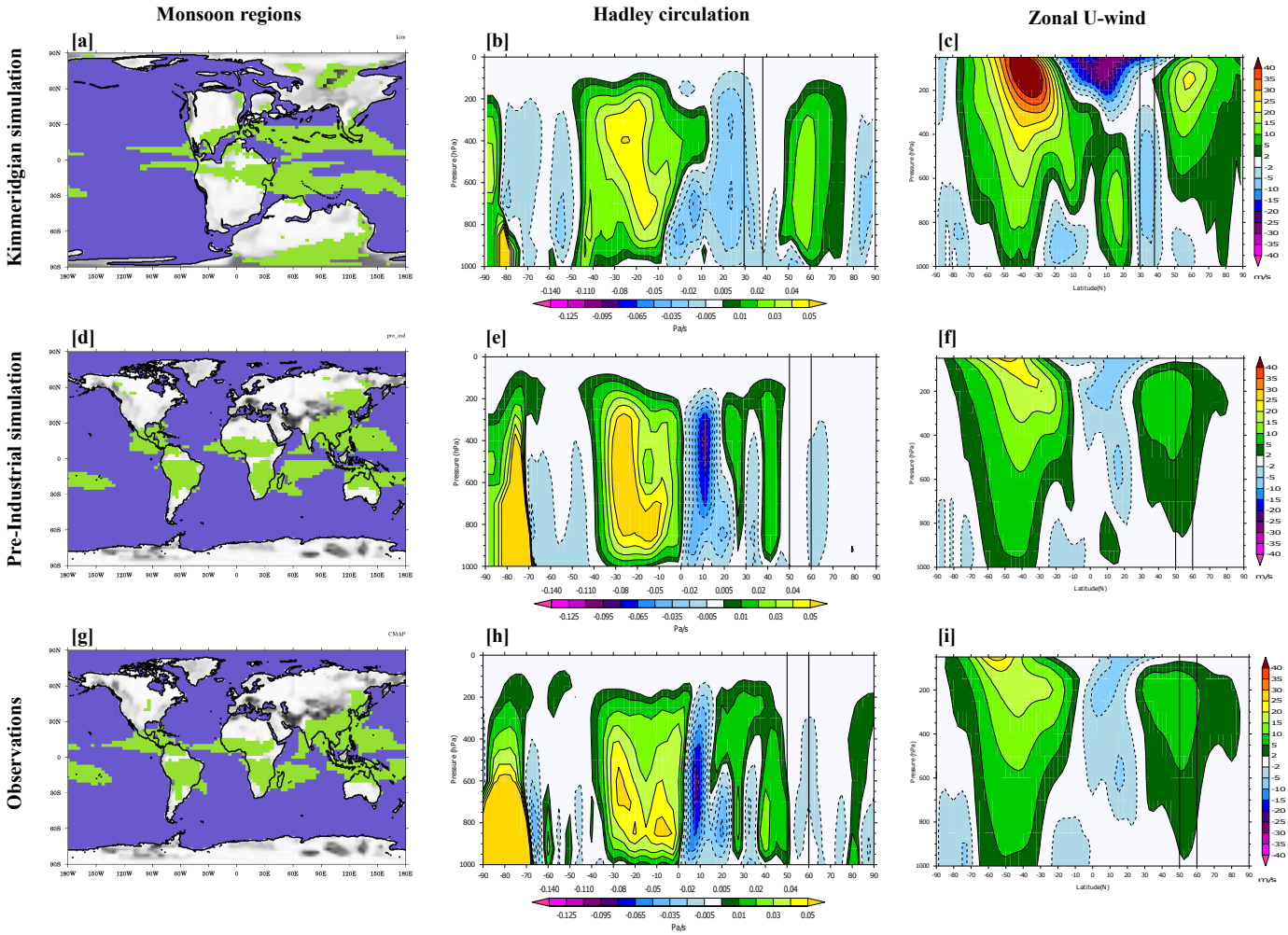
Monsoon regions
Hadley circulation
Zonal U-wind
Kimmeridgian simulation
Pre-Industrial simulation
Observations
[a]
[b]
[c]
[d]
[e]
[f]
[g]
[h]
[i]
Pressure (hPa)
Latitude(N)
Pa/s
m/s

Ammonite Zone and astrochron age
Bed group
Graphic Log
TOC (%) Interpreted 405-Kyr cycles (m)
$\delta^{13}C_{org}$
Kaolinite/Illite
Linear sedimentation rate (cm/ka)
Bulk accumulation rate (g/m²/a)
Carbonate free %TOC
Data
5 pt moving ave.
Tithonian (part)
Upper Kimmeridgian
Kimmeridge Clay Formation
147.20 Ma
fittoni
147.81 Ma
rotunda
148.36 Ma
pallasioides
148.85 Ma
pectinatus
149.45 Ma
hudlestoni
149.93 Ma
wheatley
150.1 Ma
scitulus
150.35 Ma
elegans
150.52 Ma
151.38 Ma
autissio-dorensis
eudoxus
152.76 Ma
mutabilis
153.57 Ma
cymodoce
153.93 Ma
baylei
BB2
FWS
WSB
BasSB
SJC
RLH
BSB
CHSB
GLSB
CLSB
YL
Bb42
MLSB
WLSB
TFSB
D
C
B
A
MSB
coccoliths
47.18m
84.6
110.2
130.1
162
191.2
223.5
265.1
307.4
336.9
361.7
401
429.5
464.7
501.9
536.3
564.3
mean
1-4
Carbon isotope excursion
50
100
150
200
250
300
350
400
450
500
550
Lithology
siltstone
bivalves common
nodules
dolomitic mud/siltstone
coccolith limestone
boundary uncertain
medium grey
dark grey
dark grey -black

a)

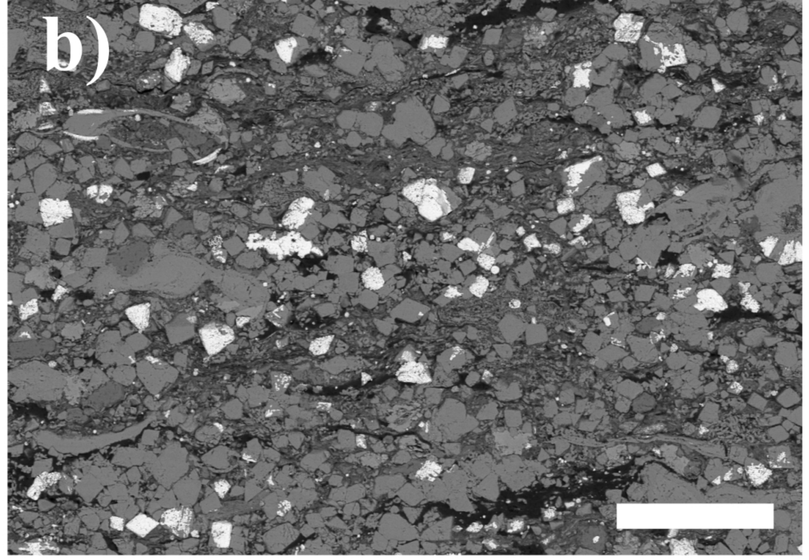
b)

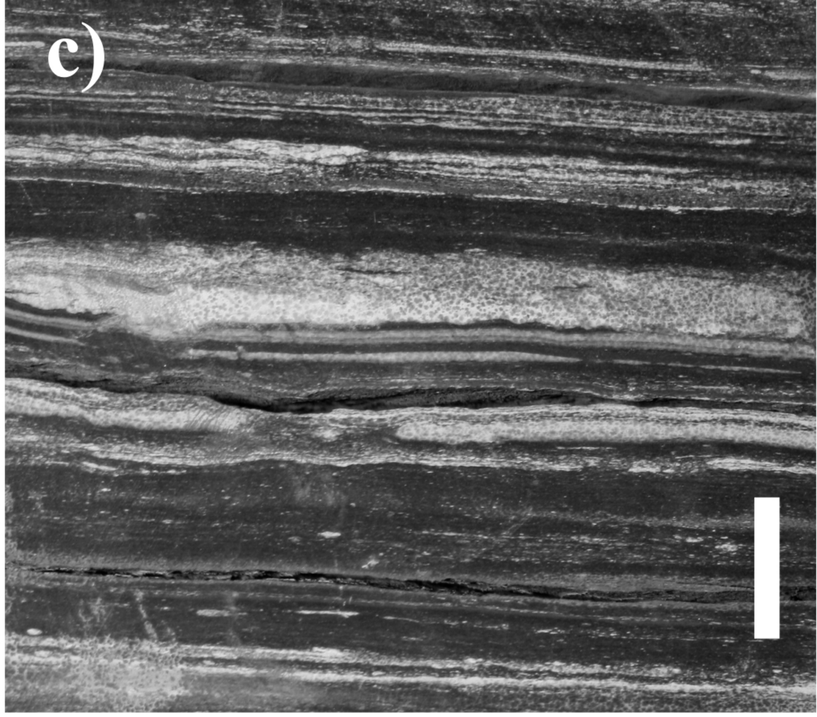
c)

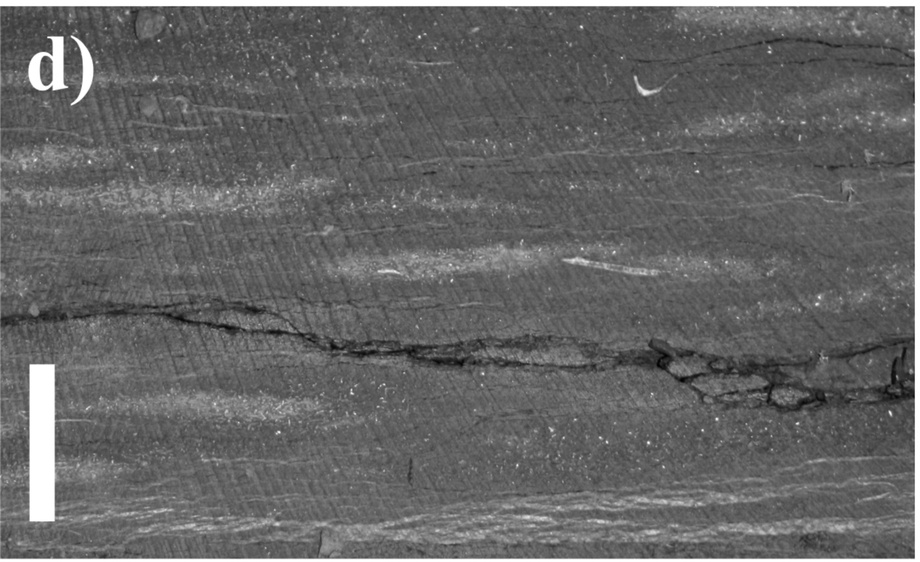
d)

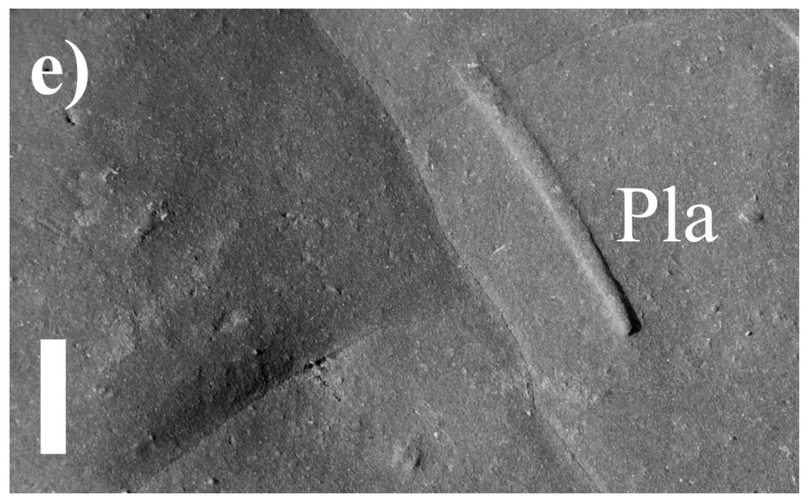
e)
Pla

f)
Rhz

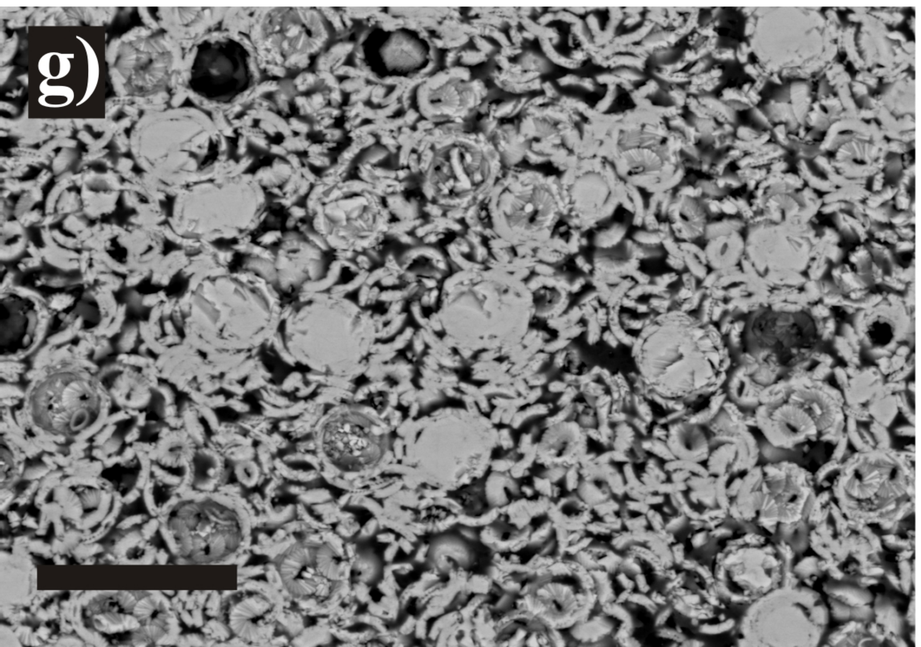
g)

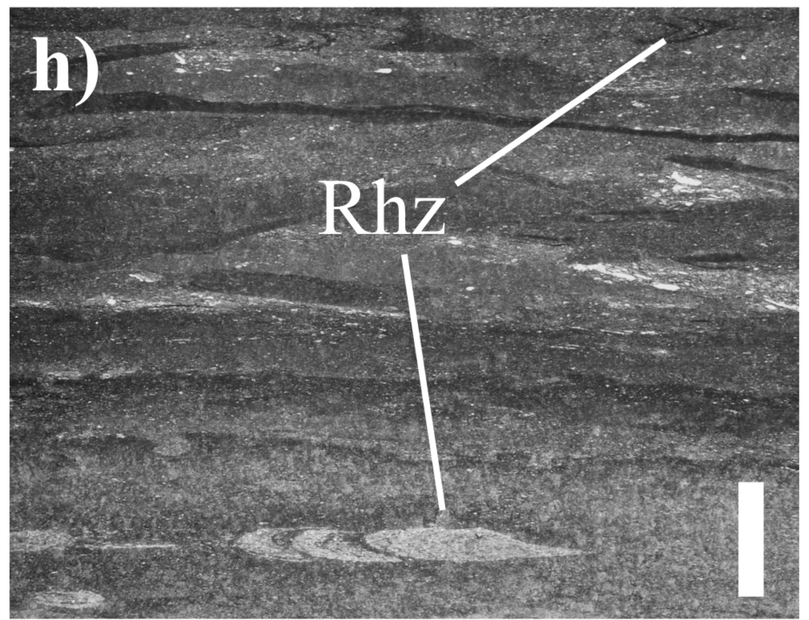
h)
Rhz

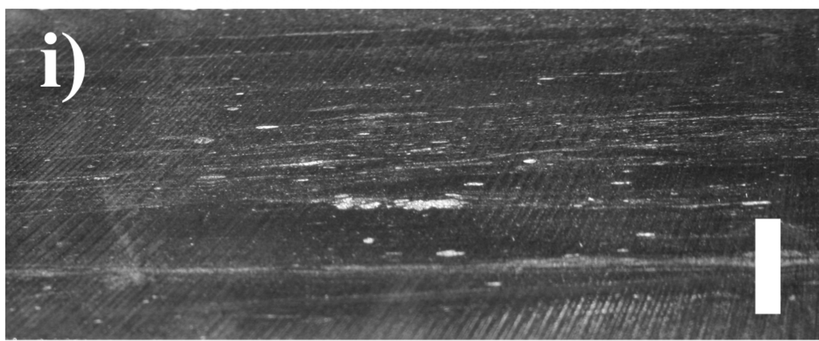
i)

Créche section, Boulonnais, northern France

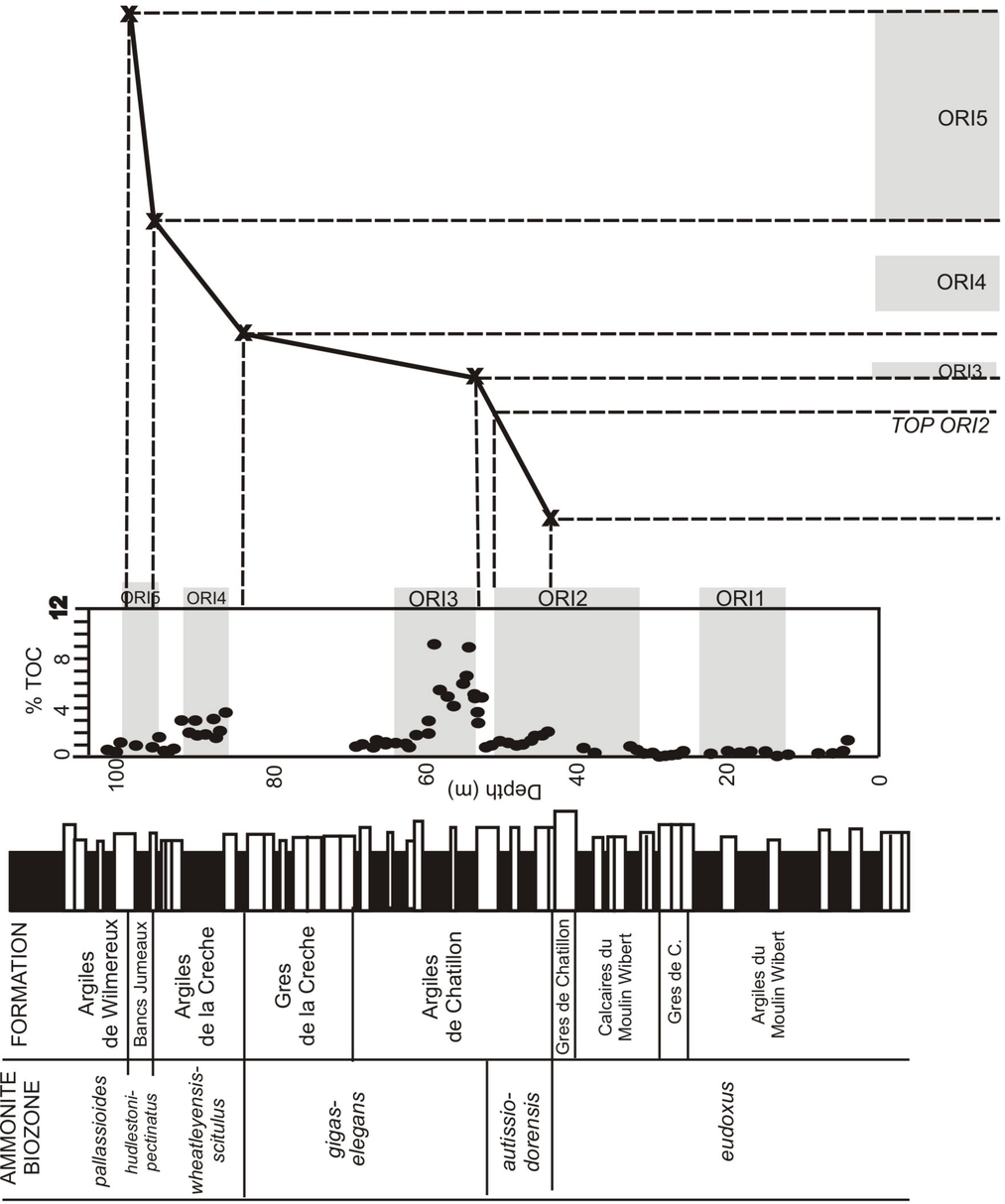

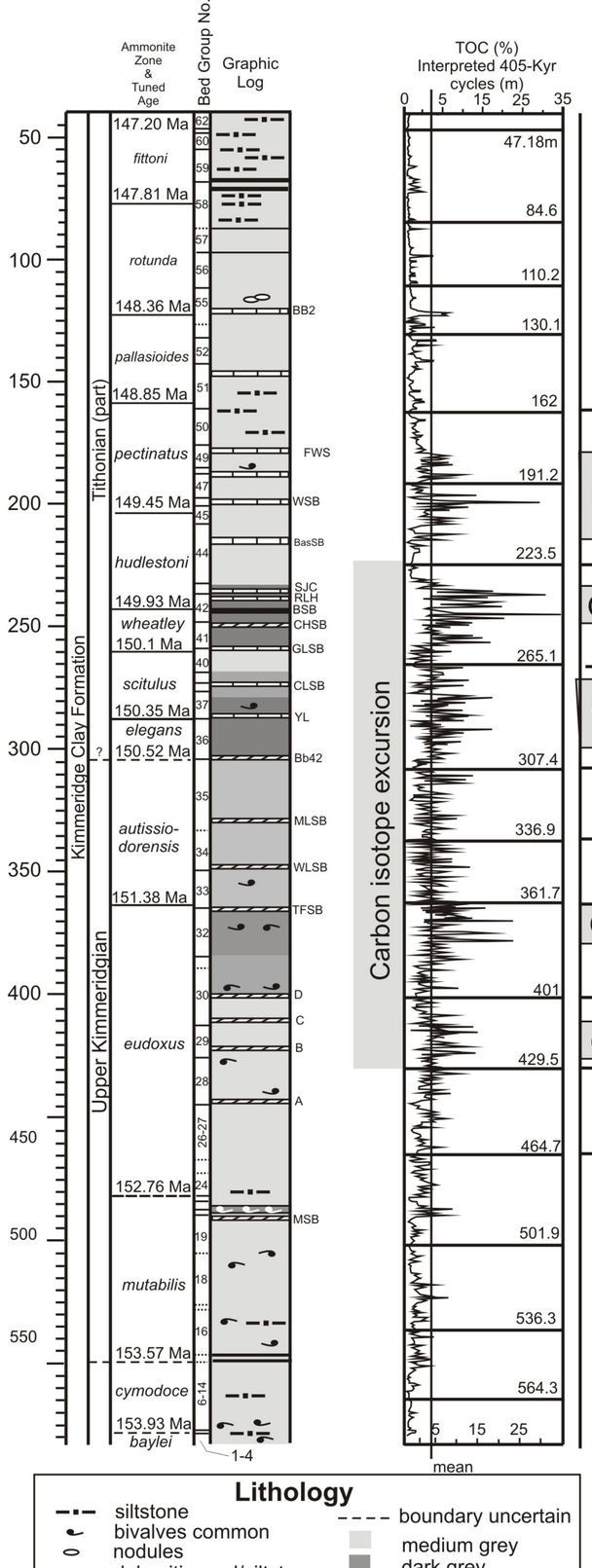

EBBERSTON 87-87 core, Vale of Pickering, Yorkshire

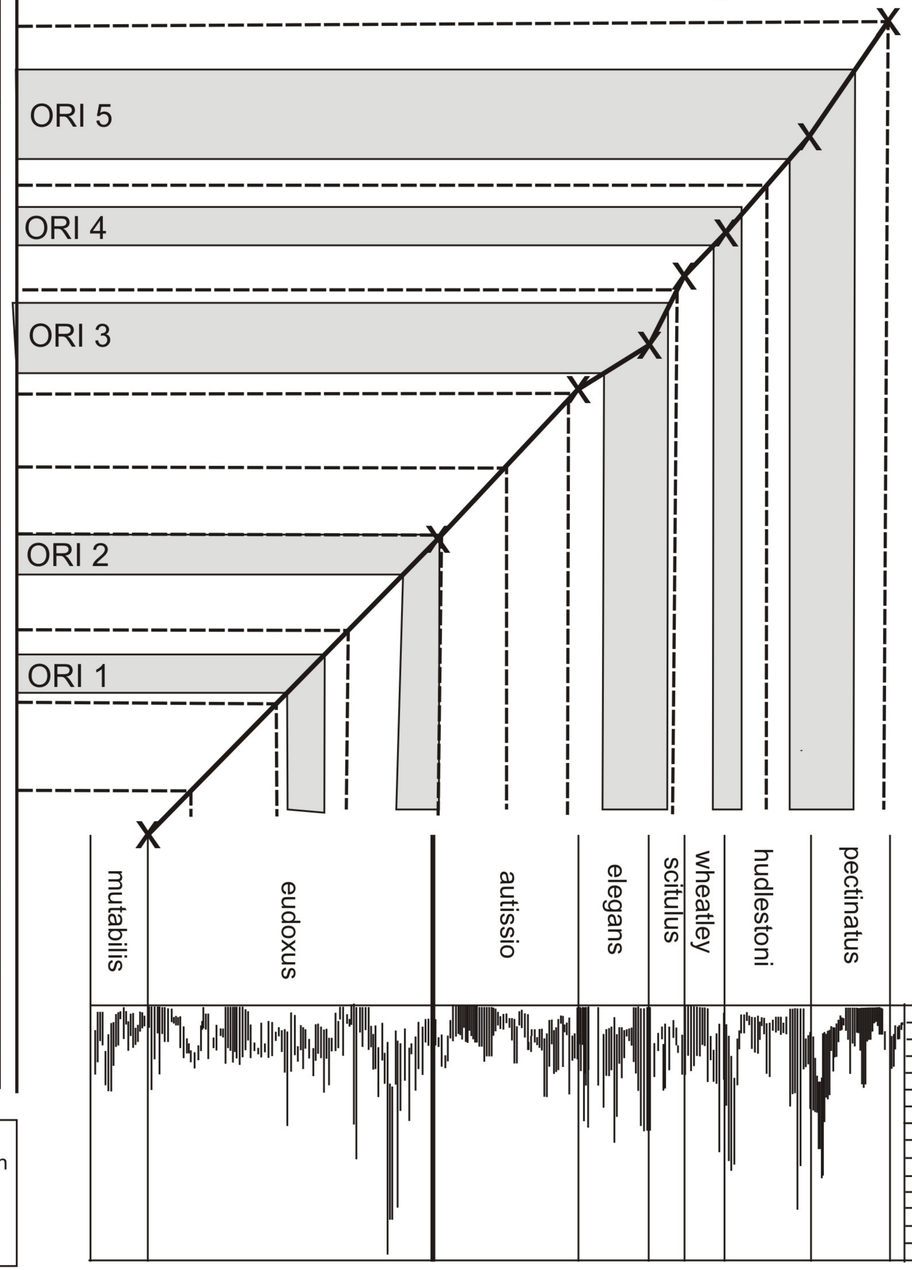

Lithology

- siltstone
- bivalves common
- nodules
- dolomitic mud/siltstone
- coccolith limestone
- boundary uncertain
- medium grey
- dark grey
- dark grey -black

400-kyr cycles with four kaolinite/illite peaks

Kaolinite /illite (solid)

%TOC carbonate-free

Depth (m)

400-kyr cycles

[Paleoceanography]

Supporting Information for

[Hadley circulation and precipitation changes control black shale deposition in the Late Jurassic Boreal Seaway]

[Howard A. Armstrong[1], Thomas Wagner[2], Liam G. Herringshaw[1, 3], Alex Farnsworth[4], Daniel J. Lunt[4], Melise Harland[5], Jonathan Imber[1,] Claire Loptson[4], Elizabeth Atar[1]]

[[1] Durham University, Department of Earth Science, Lower Mountjoy, South Road, Durham DH1 3LE, UK.

[2] Lyell Centre, Heriot-Watt University, Edinburgh, EH14 4AS, United Kingdom

[3] Department of Geography, Environmental and Earth Sciences, University of Hull, Hull, HU6 7RX, UK.

[4] School of Geographical Sciences and the Cabot Institute, University of Bristol, University Road, Bristol, BS8 1SS, UK.

[5] Getech, Kitson House, Elmete Hall, Elmete Lane, LEEDS, LS8 2LJ, UK.]

Contents of this file

Figures S1 to S2

Additional Supporting Information (Files uploaded separately)

Table S1 (3 pages, upload as separate file)

Introduction

[This Supporting Information contains i) mean precipitation (mm/s) from our model simulation of the Kimmeridgian, ii) mean precipitation (mm/s) from our model simulation

of the Modern and iii) data compiled from www.earth.ox.ac.uk/~rgge/data.html and used to calculate LSR, MAR and %TOC-carbonate free]

Kimmeridgian Precip JJA

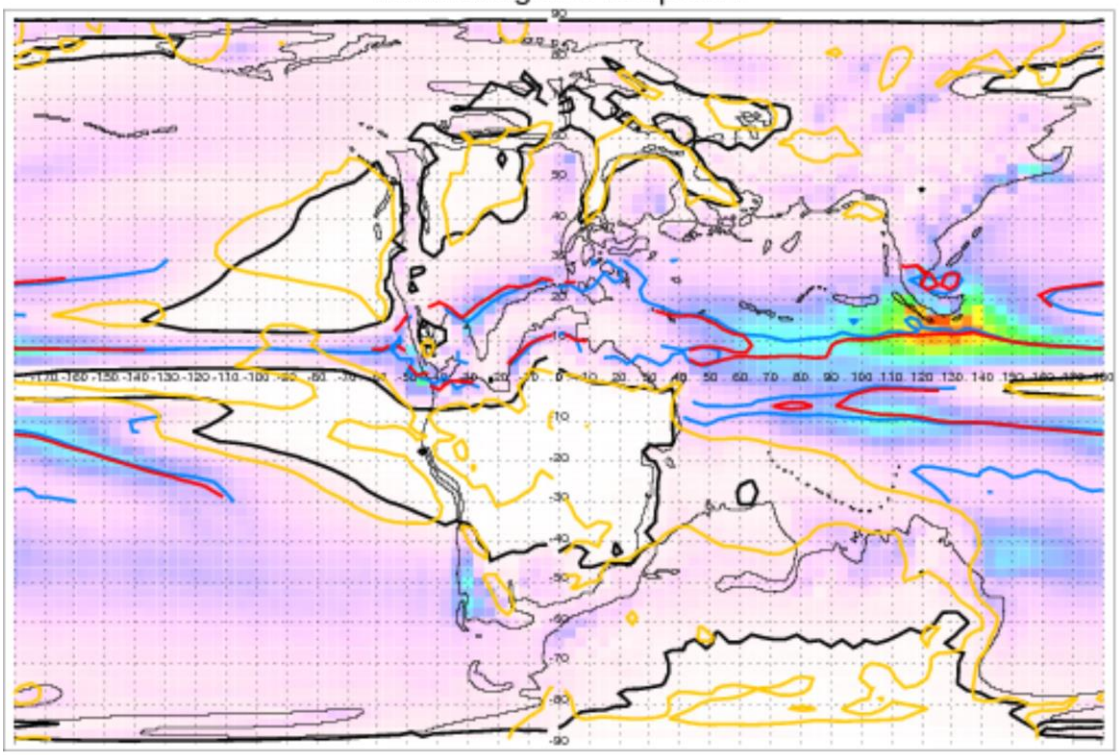

Kimmeridgian Precip DJF

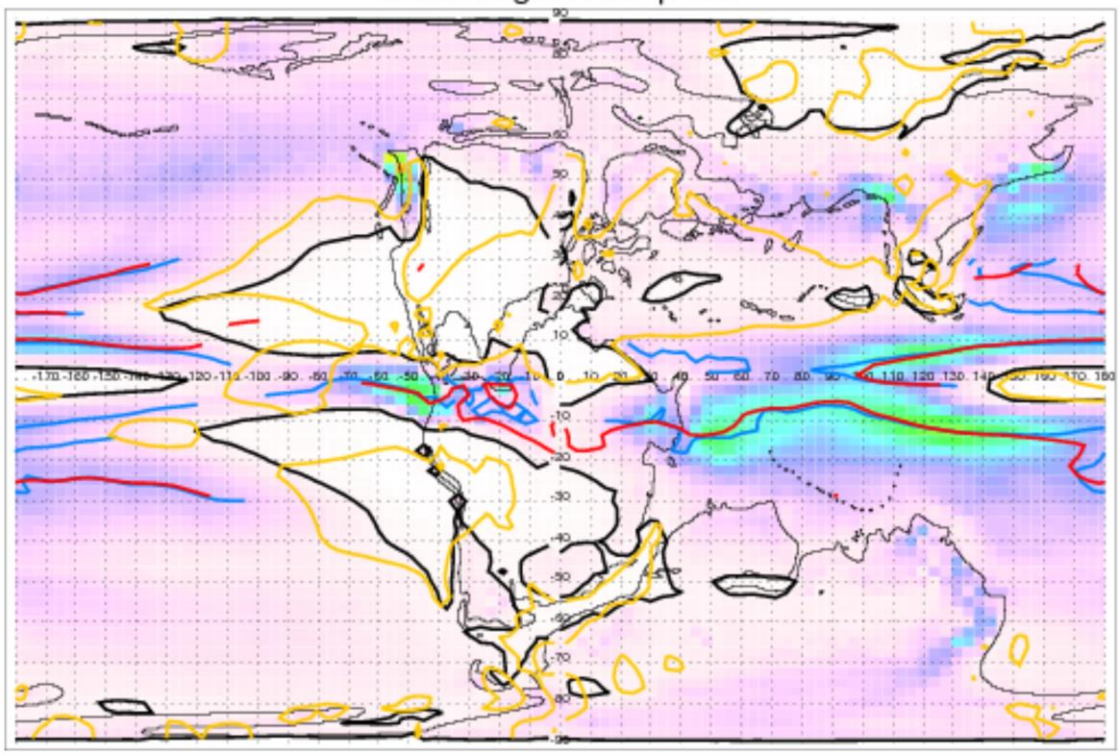

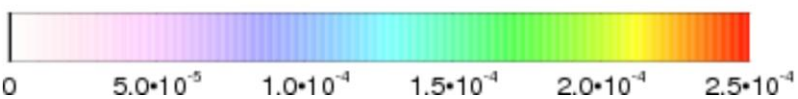

<

>

Figure S1. Upper map shows June/July/August (JJA) and lower map December/January/February (DJF) mean precipitation (mm/s) from our model simulation of the Kimmeridgian. Overlain, the red lines show the local maximum in vertical atmospheric ascent velocity (w) at a height of 500 mbar, for regions equator-wards of 30 degrees N/S, with 500 mbar temperature of greater than 260 K, and w>0.005 m/s. The blue lines show the local maximum in precipitation (p), for regions equator-wards of 30 degrees N/S, with 500 mbar temperature of greater than 260K, and p>0.00003 mm/s. Thick black line encompasses dry regions where the precipitation rate is less than 1*10^{-5} mm/s. The orange line encompasses regions of mid-atmospheric descent where the vertical velocity at 500 mbar is towards the surface and greater than 0.02 is m/s.

Modern Precip JJA

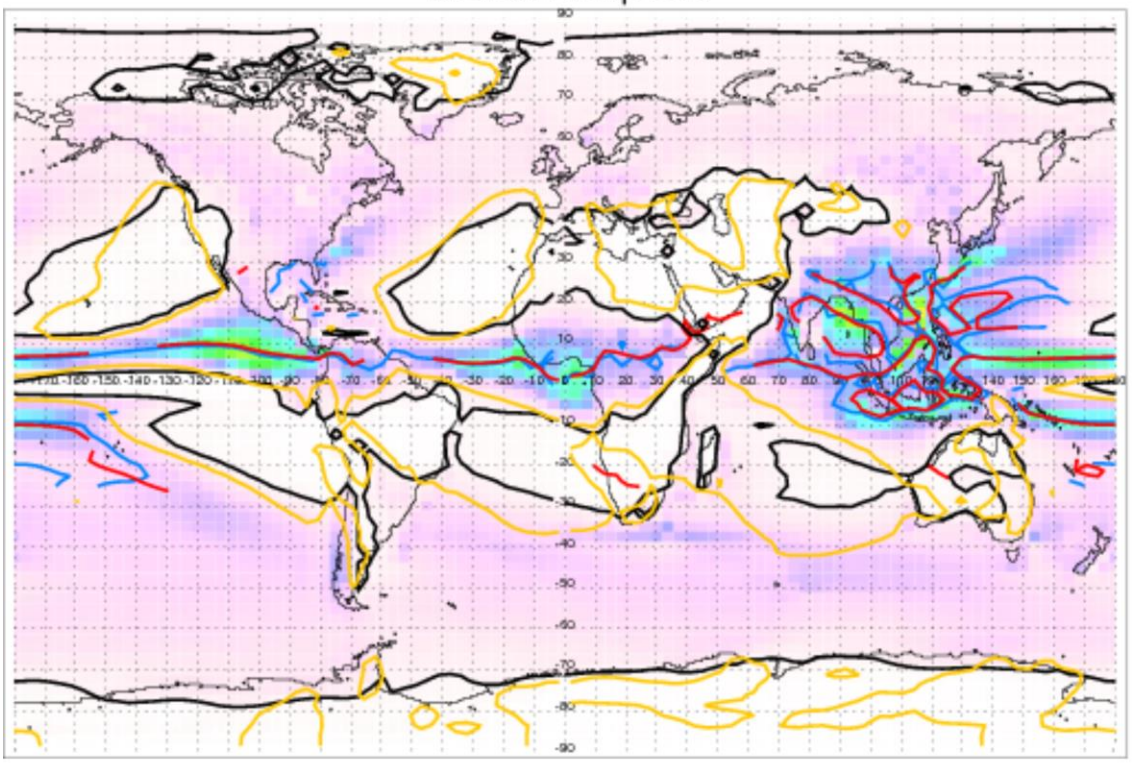

Modern Precip DJF

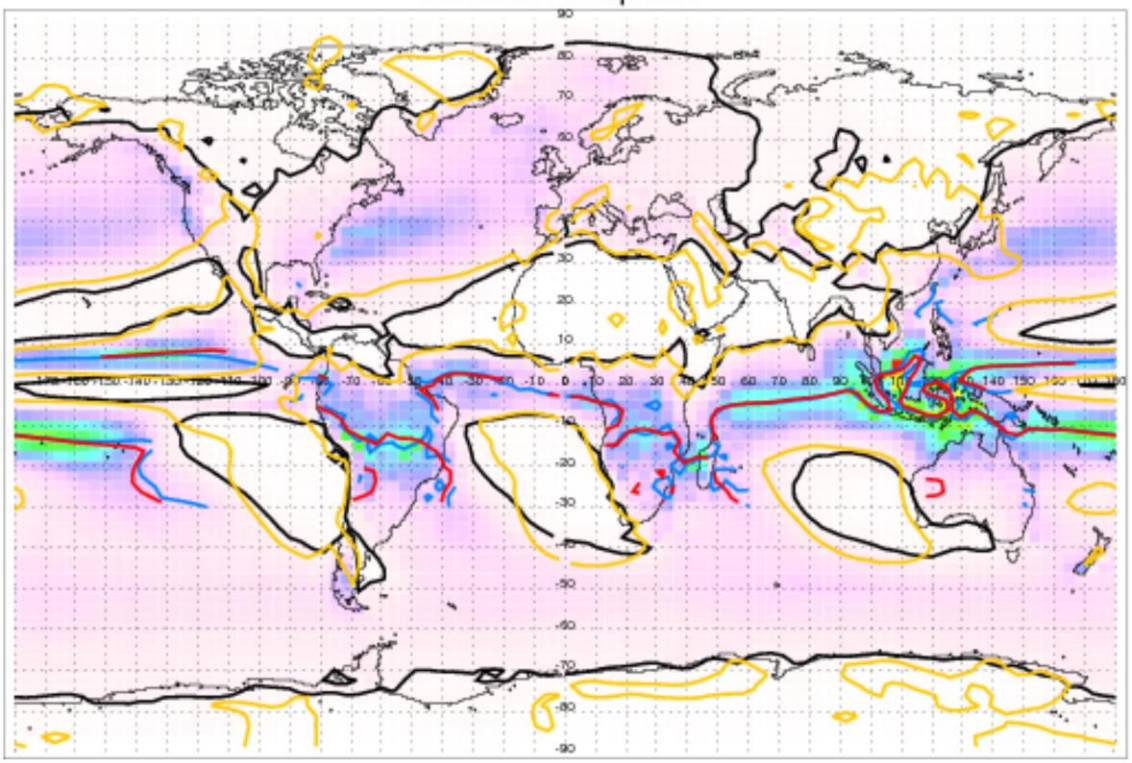

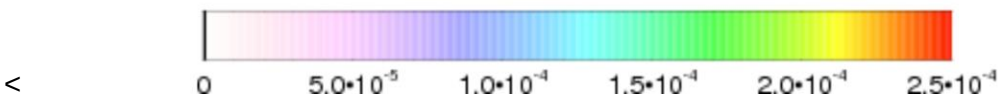

>

Figure S2. Upper map shows June/July/August (JJA) and lower map December/January/February (DJF) mean precipitation (mm/s) from our model simulation of the Modern. Legend is as for Figure S1.

Table S1. Compilation of data (from *Morgans-Bell* et al. [2001], www.earth.ox.ac.uk/~rgge/data.html), linear sedimentation rate (LSR) and and mass accumulation rate (MAR) results. (3 pages, uploaded as separate file).